SELF-HEALING COATINGS FOR STEEL REINFORCED INFRASTRUCTURE

by

Adrienne Weishaar

A Thesis

Submitted to the Faculty

of the

WORCESTER POLYTECHNIC INSTITUTE

in partial fulfillment of the requirements for the

Degree of Master of Science

in

Civil Engineering

April 2018

APPROVED:

Dr. Aaron Sakulich, Major Advisor

Dr. Leonard Albano, Committee Member

Dr. Rajib Mallick, Committee Member

Dr. Amy Peterson, Committee Member

Abstract

Epoxy coatings are currently the most popular corrosion protection mechanism for steel reinforcement in structural concrete. However, these coatings are easily damaged on worksites, negating their intended purpose. This study investigates self-healing coatings for steel reinforcement to introduce an autonomous healing mechanism for damaged coatings. Coatings were applied to steel coupons, intentionally damaged, and introduced to a corrosive environment via aerated salt-water tanks. Performance of the experimental coatings was evaluated qualitatively and quantitatively. Adhesion strength and effects of coating thickness were also studied. Results from coated steel coupons subjected to damage and submerged in salt-water aeration tanks exhibited improved corrosion resistance performance with self-healing coatings. However, self-healing coatings have comparable poor adhesion to the substrate as do conventional coatings. This paper shows preliminary results demonstrating the potential benefits of self-healing coatings for steel reinforcement and identifies numerous avenues for future research.

Acknowledgments

I want to thank my advisor, Professor Aaron Sakulich, for all of his guidance and time in completing this research. I would also like to thank Professor Amy Peterson for allowing me to utilize her lab space and for her time and guidance. Additionally, thank you to Dr. Boquan Li for taking the time to teach me how to use Scanning Electron Microscopy, Professor Marion Emmert and her postdoc, Remya Narayanan, for allowing me to use her lab space and assisting me during my cement forensics research, and Professor Leonard Albano for always offering his time and assistance throughout my entire educational career at WPI.

Table of Contents

Table of Figures

List of Tables

1.0 Introduction

Structural concrete is one of the most widely used infrastructure materials in the U.S. Currently 3.2 billion yd^3 (7 billion m^3) of structural concrete are in place in the United States and 497 million yd^3 (380 million m^3) more are added each year [1]. That's equivalent to over 2,000 Empire State Buildings currently filled with structural concrete and over 360 more filled each year. Of the 615,002 bridges in the United States, approximately one third are constructed with structural concrete [2]. However in 2017, the American Society of Civil Engineers (ASCE) assessed America's infrastructure based on capacity and condition, among other key criteria, and assigned a grade of "D+." Specifically, U.S. bridges were graded as "C+." This score represents infrastructure that is in substandard condition, exhibits significant deterioration, and has a high risk of failure [3]. Additionally, the ASCE estimates that $4.59 trillion are needed by 2027 to rehabilitate and improve the condition of U.S. infrastructure. Furthermore, the ASCE recommends key solutions such as supporting research and development of innovative materials to extend the service life of infrastructure [3].

Steel reinforced concrete, also known as structural concrete, was first adopted in the United States in 1889 for the construction of the Alvord Lake Bridge in San Francisco, CA (Figure 1) [1]. Since then, structural concrete was rapidly adopted as a building material. However, by the mid 1970's researchers recognized that the deterioration of bridge decks coincided with locations of deicing salt application and attributed this degradation to corrosion of the steel reinforcement caused by the ingress of chloride ions (Figure 2) [4].

Figure 1: The Alvord Lake Bridge, the first bridge in the U.S. constructed with structural concrete [5].

Figure 2: Corrosion of steel reinforcement on the bridge deck of the Devil's Elbow Bridge in Missouri [6].

The most common corrosion protection method is the application of fusion bonded epoxy (FBE) coatings to rebar [7]. Fusion Bonded Epoxy (FBE) is applied to reinforcing steel before it is placed in concrete to delay the onset of corrosion. The FBE process uses an electric field to distribute a powder composed of epoxy resin, a curing agent, and other additives onto heated steel, where the powder melts and chemically reacts to form an impenetrable coating. Since the adoption of epoxy coated rebar in the 1970's, the Federal Highway Administration (FHWA) estimates that billions of dollars have been saved in rehabilitation costs [5].

FBE coatings have proven successful in delaying the onset of corrosion; however, the brittle coatings are easily damaged during worksite handling, negating their intended purpose. Self-healing coatings have the potential to be an improved mechanism, compared to conventional FBE coatings, to inhibit deterioration of modern infrastructure. Self-healing coatings autonomously "heal" at damage locations and continue to protect the substrate from corrosive media. Coatings that initiate self-healing in response to external damage have seen substantial research for anti-corrosion applications [8][9][10], but have only recently been investigated for structural concrete systems [11].

In accordance with the ASCE recommendation to "investigate innovative new materials"[3], this research explored augmenting current FBE coatings with poly(urea-formaldehyde) microcapsules containing tung oil to create self-healing coatings. This work further assessed the effectiveness of self-healing coatings under damaging conditions to evaluate the self-healing capacity of the coatings. To this end, self-healing coatings were applied to steel coupon samples that were then damaged and submerged in aerated salt-water baths for accelerated corrosion testing.

2.0 Background

2.1 Steel Reinforced Infrastructure

Structural concrete is a commonly used construction material. Concrete and steel complement each other, with concrete resisting compressive forces while steel resists tensile forces. Without steel, concrete has minimal tensile capacity. Steel reinforcement, also known as rebar, was incorporated in structural designs as early as 1854 in France. However, a patent for the invention of reinforced concrete wasn't obtained until 1867 for garden pots and planters. By 1873, reinforced concrete was patented again for use in water tanks and bridges, and once more in 1877 for beams and columns [12].

The United States adopted reinforced concrete as a building material in 1875. In 1877, Thaddeus Hyatt published results of flexural tests using reinforced concrete. His findings established the principles for the analysis and design of reinforced concrete. Throughout the remainder of the late 1800's, reinforced concrete was used for walls, beams, slabs, columns, and staircases, among other structural components. Furthermore, houses, museums, buildings, and bridges were designed and constructed using reinforced concrete. By 1906, the French Ministry of Public Works established and published specifications for reinforced concrete. Throughout the 1900's research and use of reinforced concrete continued [12].

However, by the 1960's, steel reinforced concrete bridges began to display problems such as delamination and spalling in coastal regions. At this time, people began to recognize the degradation of bridge decks in snowy regions with the increased application of deicing salts in the winter months [7]. By the mid 1970's, researchers identified rebar corrosion as the primary cause of degrading bridge decks.

Today, research continues to develop applications and designs of reinforced concrete, as it has become one of the most popular building materials. Reinforced concrete is desirable as it is readily available, easily molded into any shape, cost effective, and is inherently rigid and fire-resistant. However, steel reinforcement needs to have adequate protection to ensure these characteristics.

2.2 Corrosion Process

Steel has many different chemical compositions with varying elemental quantities depending on its intended use. The main element of steel is iron. Iron in its natural state is iron ore. It is derived from its ore state by a process known as smelting in which the metal absorbs and retains the energy needed to free it from the ore. In this state, the unstable metal commonly reacts with elements in the environment and returns to iron ore, expelling the extra energy. This process is known as oxidation, or corrosion. The rate of corrosion of steel in concrete depends on the availability of air, water, and aggressive ions. Furthermore, the corrosion rate is influenced by environmental factors such as temperature and pH, and by material properties such as composition, grain structure, and internal stresses [5].

Corrosion of steel reinforcement is a product of many processes beginning with the initial concrete-reinforcement bond. Due to the high pH of concrete, an oxide film forms on the surface of the embedded steel, creating a passive layer, and preventing the anodic dissolution of steel. However, chloride ions permeate through the concrete and deteriorate this protective film initiating the corrosion process. Without chloride ions, steel reinforcement does not typically corrode [13].

Once the passive layer is destroyed, three processes can summarize the corrosion of steel in concrete. First, a depolarization reagent, such as oxygen, arrives at the surface of the metal after diffusing through the concrete. Then, electrochemical reactions occur at the interface between the steel and concrete. Lastly, rust, a reaction product, accumulates on the surface of the metal (Figure 3) [14].

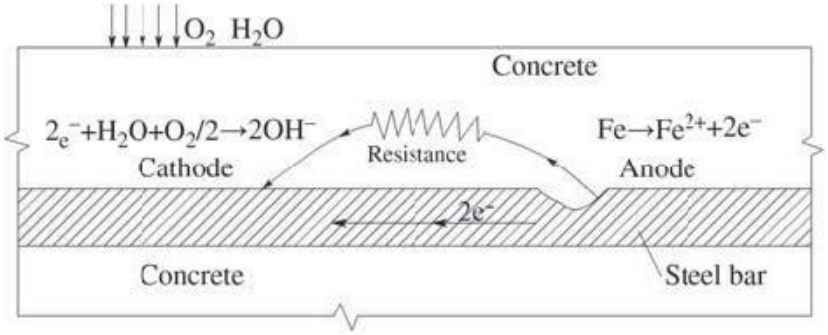

Figure 3: Representation of corrosion of steel in concrete [13].

An anodic reaction occurs at the anodic site, labeled in Figure 3. This reaction releases electrons and oxidizes iron into the ferrous state:

$$Fe \rightarrow Fe^{2+} + 2e^{-} \quad (1)$$

Oxygen easily diffuses through concrete as a depolarization reagent. At the cathodic site in Figure 3, an electrochemical reaction reduces oxygen into hydroxide ions:

$$O_2 + 2H_2O + 4e \rightarrow 4OH^{-} \quad (2)$$

The two products of the equations above, ferrous ions and hydroxide ions, combine to produce ferrous hydroxide:

$$Fe^{2+} + 2OH^{-} \rightarrow Fe(OH)_2 \quad (3)$$

Ferrous hydroxide continues to oxidize with moisture, forming ferric oxide, more commonly referred to as rust [14]:

$$4Fe(OH)_2 + 2H_2O + O_2 \rightarrow 4Fe(OH)_3 \quad (4)$$

$$2Fe(OH)_3 \rightarrow Fe_2O_3 + 3H_2O \quad (5)$$

The production of rust from the corrosion process reduces the cross-sectional area of the reinforcement, directly affecting the load capacity. Furthermore, the rust occupies a volume greater than the original reinforcement, causing internal stresses in the concrete, leading to cracking and eventual loss of concrete cover (Figure 4). Damage of the concrete surrounding steel reinforcement exposes larger regions of steel to the corrosive environment, causing more corrosion to occur.

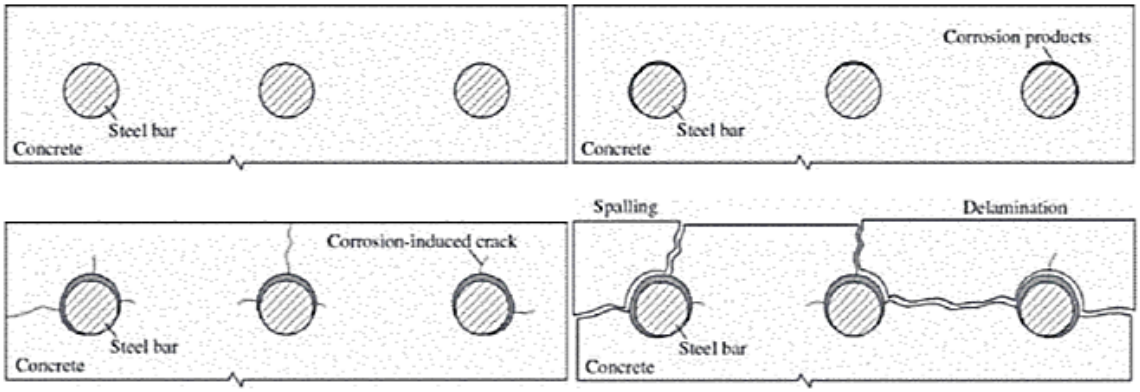

Figure 4: Diagram showing the degradation of structural concrete with corrosion of steel reinforcement [14].

2.3 Corrosion Mitigation Techniques

Reinforced concrete has many benefits that are only reaped when steel is adequately protected against corrosive forces. Methods of improving the corrosion resistance of reinforcement include increasing the concrete cover, decreasing the porosity of the concrete, and using inhibitors as admixtures in the concrete. These methods prolong the diffusion of corrosive media through the concrete and therefore delay the onset of corrosion. However, when the aggressive media arrives at the unprotected reinforcement, the steel will corrode. Therefore, these methods only have short-term effectiveness. Longer-term corrosion mitigation methods include using stainless steels, galvanized steels, or epoxy-coated steel. The following sections give an overview of these mitigation techniques.

2.3.1 Stainless Steel Reinforcement

Stainless steels are a group of alloys containing a minimum of 12% chromium and can include other various alloying agents. The addition of chromium causes a passive iron-chromium oxide film to form on the surface of the reinforcement, preventing the anodic dissolution of iron [15]. Corrosion resistance increases with an increase in chromium content. Additionally, other alloys such as nickel can be added to change the mechanical properties and corrosion behavior of the metal [16].

There are three main types of stainless steel used for reinforcement including ferritic, austenitic, and ferritic-austenitic. Ferritic steels are low carbon plain chromium steels with less than 17% chromium content. Austenitic steels are low carbon steels with 18% chromium and 8% nickel. Ferritic-austenitic steels are 22-28% chromium and 4-8% nickel. The degree of corrosion protection, mechanical properties, workability, and cost varies with different chromium and nickel content. These variables come into consideration when designing with stainless steel reinforced concrete [16].

While stainless steel is one of the most effective corrosion mitigation measures, it has a relatively high associated cost. Depending on the composition of the stainless steel, ‘as rolled’ it may not provide as much strength compared to plain steel reinforcement, and therefore require heat treatment or cold working to improve the mechanical properties [7] (Figure 5). These processes cause stainless steel to be more expensive. Additionally, the cost of stainless steel increases with alloying content. Therefore, the cost of stainless steel increases with an increase in desired corrosion resistance [16]. This factor limits the use of stainless steel in reinforcement to critical components and designs with a high risk of corrosion.

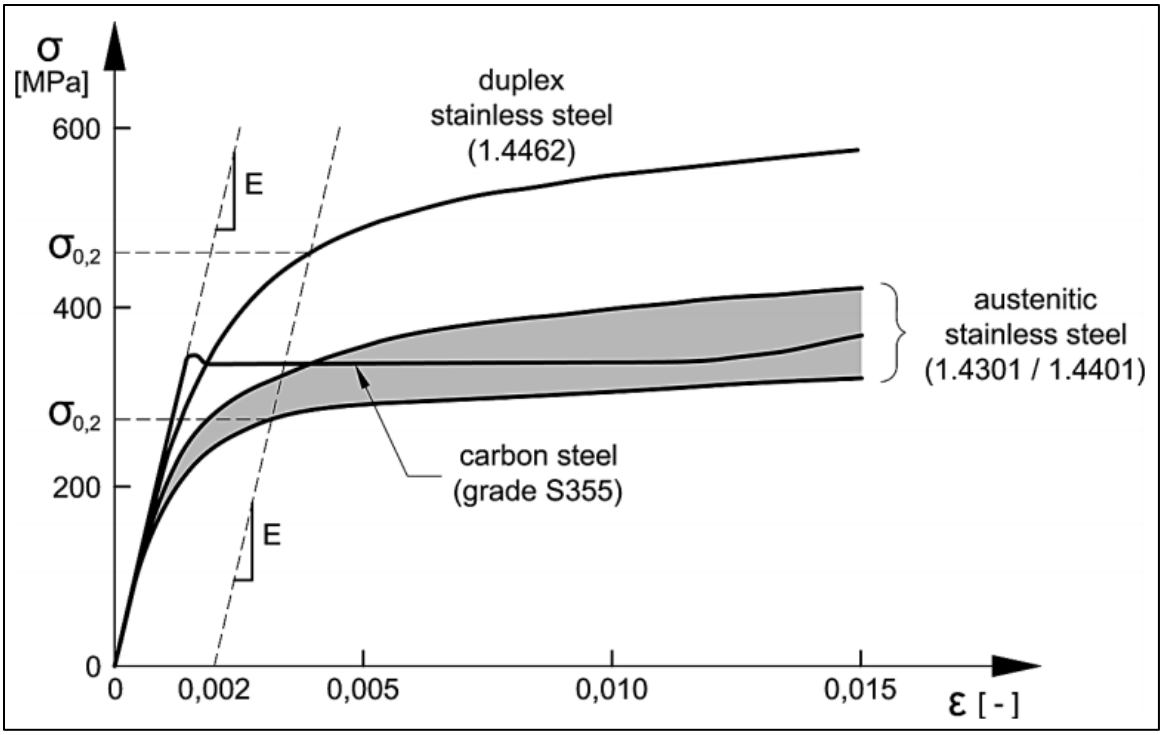

Figure 5: Stress-strain diagram comparing ferritic and austenitic stainless steels to carbon steel showing that carbon steel has a higher yield strength than austenitic stainless steel. In addition, stainless steel has a nonlinear stress-strain relationship compared to carbon steel [17].

2.3.2 Galvanized Steel Reinforcement

Galvanized steel reinforcement is another mitigation technique that utilizes a sacrificial coating to increase corrosion resistance. These zinc coatings are created by a hot-dip process in which steel reinforcement is cleaned, shot blasted, and dipped in molten zinc. After the steel is zinc-coated, the reinforcement is immersed in a chromate bath to prevent the coating from reacting before the concrete has cured [7]. Before hot-dipping, steel can be in the form of straight bars, bent, or in fabricated networks. Zinc has a higher chloride concentration threshold for corrosion than steel, delaying the onset of corrosion. Additionally, if these coatings crack, zinc, having a more negative corrosion potential than steel, will corrode before the reinforcement. When the zinc corrodes, it forms a hydrated oxide layer that acts as a barrier at corrosion sites to prevent the advancement of corrosion [18].

Galvanized steel, while more expensive than plain steel reinforcement, is more cost effective than stainless steel. However, there are setbacks that prevent the widespread adoption of galvanized reinforcement in concrete. Galvanized reinforcement has diminished bond strength between the concrete and reinforcement. Additionally, galvanized steel performs well in carbonated concrete but only has limited efficiency in chloride rich environments as the chloride concentration threshold will eventually be exceeded, just at a slower rate than uncoated steel reinforcement [19].

2.3.3 Fusion Bonded Epoxy Reinforcement

Epoxy coatings are the most common corrosion protection method for steel-reinforcement in the United States. First introduced to the construction industry in the early 1970's, epoxy coatings

isolate steel from concrete by creating a barrier to chloride ions. These coatings are considered a cost-effective backup to other corrosion protection methods [7].

Fusion Bonded Epoxy (FBE) is a powder coating applied to steel reinforcement before it is encased in concrete. FBE coatings are thermoset polymers, meaning they set irreversibly. Before coating the reinforcement the bar is blasted clean to remove mill scale, rust, and contaminants. Then the bar is heated, typically to 446°F (230°C), and passed through an electrostatic spray that applies the charged epoxy powder to the steel. The epoxy melts and bonds to the bars which are then quenched with a water spray (Figure 6) [20].

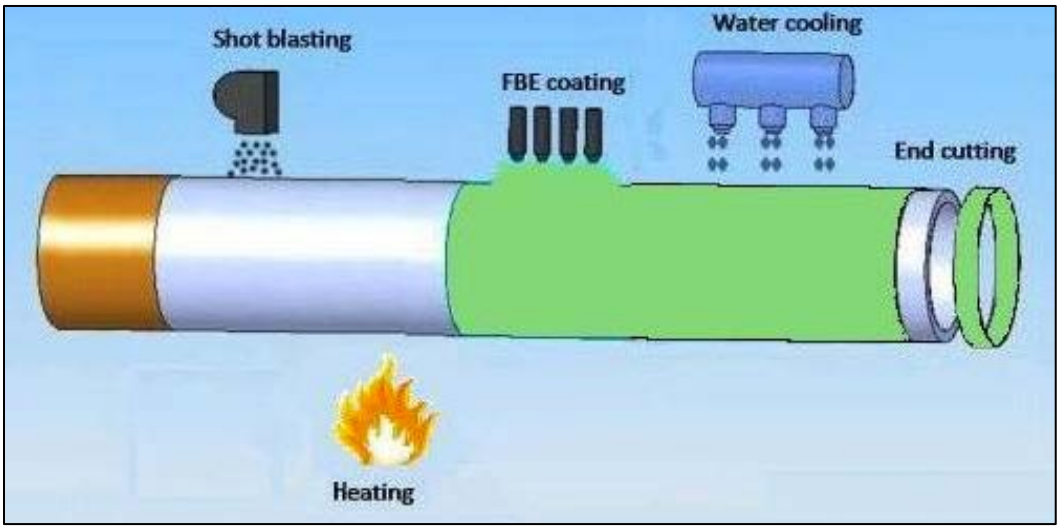

Figure 6: Manufacturing process of FBE coatings [21].

In the United States there are over 235,000 structural concrete bridges utilizing epoxy coatings [22]. Studies have shown that epoxy coated rebar is less susceptible to corrosion than uncoated rebar; however, FBE coated steel reinforcement still corrodes due to imperfect and damaged coatings [23]. Once these coatings are damaged, corrosion of the metal substrates initiates and propagates. Furthermore, similar to galvanized reinforcement, there is diminished bond strength between the concrete and reinforcement with the application of these coatings.

2.4 Self-Healing Coatings and Techniques

While there are numerous corrosion mitigation techniques for steel reinforced concrete, corrosion continues to be a cause of bridge degradation in the United States [22]. For this reason, alternative methods are being investigated to improve the current state of infrastructure. Self-healing coatings is a topic that has seen substantial research in regards to corrosion protection [8][9][10]. Self-healing epoxy coatings autonomously “heal” at damage locations. Approaches for healing functions include encapsulation, reversible chemistry, microvascular networks, nanoparticle phase separation, and hollow fibers [24](Table 1).

Table 1: Explanation of various self-healing mechanisms.

Self-Healing Mechanism	Explanation
Encapsulation	Solids, liquids, or gases encased in shells to isolate the encapsulated agent from the external environment. When the shell is damaged or ruptures, the core substance is released to "heal" the damaged region [25].
Reversible chemistry	A mechanism utilizing thermally reversible reactions for multiple healing cycles. Catalysts are incorporated into a coating and upon damage, the released reactants cure the damaged area [26][27].
Microvascular networks	Networks, similar to biological vascular systems, that are filled with a liquid healing agent. Damage to the network releases the liquid to induce self-healing and repair [28].
Nanoparticle phase separation	Particles with small diameters, in between the solid and molecular states with phase diagrams different than that of the bulk materials. These nanoparticles are incorporated into materials and act as patches at damaged locations [29][30].
Hollow fibers	Hollow capillaries filled with a curing agent. This mechanism contains more healing agent and allows for larger, repetitive damage [25].

Microencapsulation is of particular interest for the proposed research. This approach incorporates a core-shell microparticle into the epoxy matrix. When the epoxy coating is damaged, these microcapsules rupture and release the core substance, which oxidizes on the surface of the metal to form an impenetrable barrier (Figure 7).

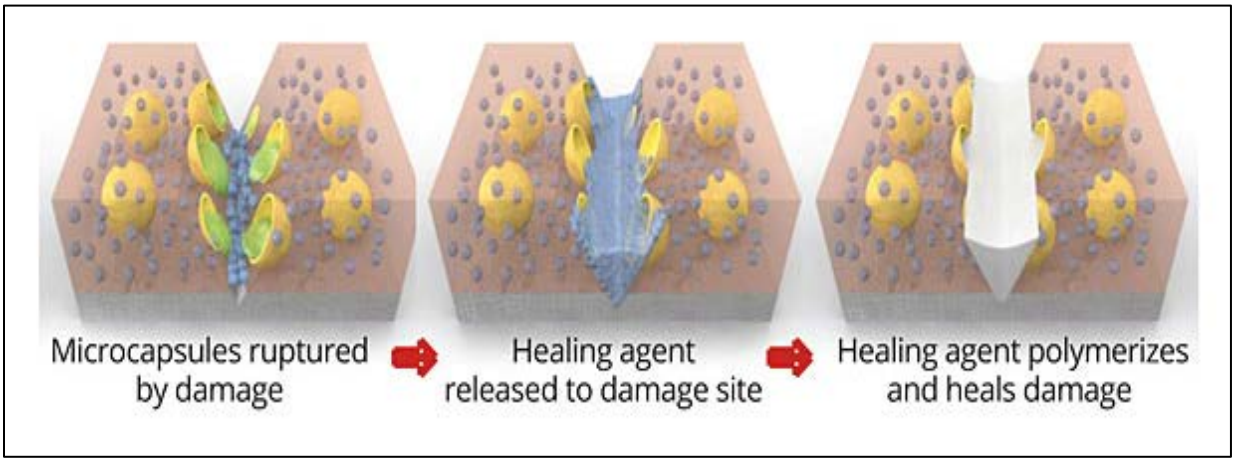

Figure 7: Concept of self-healing coatings with microcapsules [24].

Incorporating healing mechanisms into epoxy coatings has the potential to improve coating performance. Adapting these coatings for steel reinforcement could eliminate, or considerably delay, the onset of corrosion in steel reinforcement, improving the condition of structural concrete, resulting in improved infrastructure health.

2.5 Previous Research on Self-Healing Coatings for Reinforcement

Chen *et al.* published preliminary studies of self-healing coatings for steel reinforcement [11]. In this investigation, tung oil was encapsulated through an emulsion process. Tung oil is a triglyceride drying oil, primarily consisting of alpha-eleostearic acid. When the tung oil is exposed to air, from the rupturing of the microcapsules, the drying oil polymerizes via an autocatalytic oxidation reaction. This creates a hard, water proof coating [11]. Microcapsules filled with tung oil were incorporated into an epoxy matrix, creating an experimental self-healing coating. These coatings, along with conventional epoxy, were applied to steel reinforcement and given several days to cure. After curing, samples were damaged and embedded into concrete. Accelerated corrosion testing was utilized to assess and compare the corrosion resistance of the experimental and control samples.

Control and experimental samples were damaged by cutting and impacting, in order to test the self-healing ability. Upon cut damage, and in the following days, images were taken by optical microscope that confirmed the self-healing ability of the experimental coatings (Figure 8). Impact damage was more severe for experimental coatings than for control coatings: experimental coatings debonded and delaminated at and surrounding impact locations, whereas control coatings only debonded at the impact location. This result suggested that the incorporation of microcapsules could diminish the adhesion strength of self-healing coatings [11].

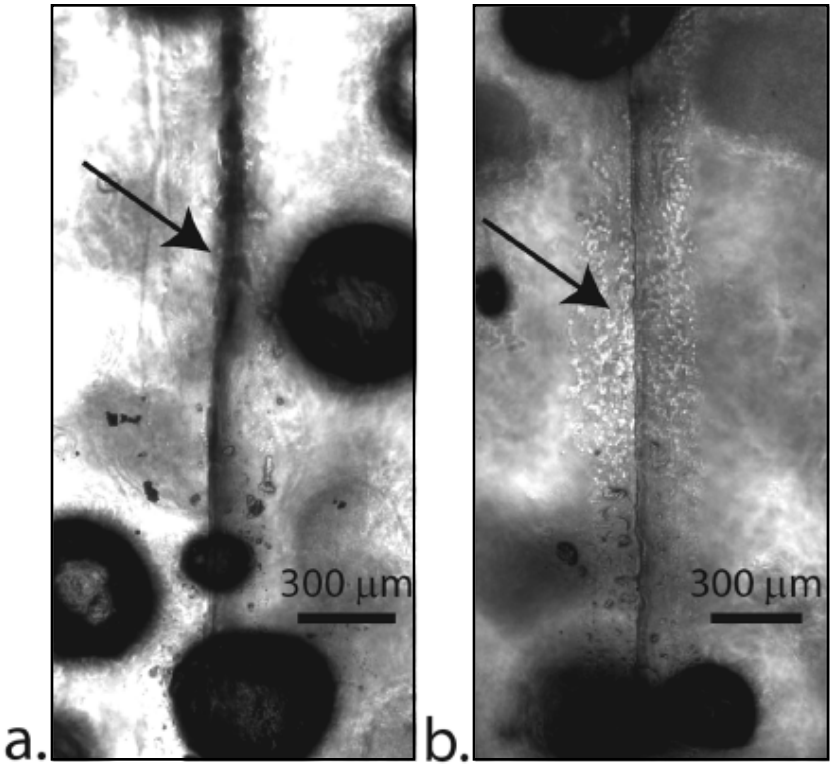

Figure 8: Results from Chen *et al.* displaying the initial cut made in a self-healing coating (a) and the cut healed after 5 days (b), suggesting the efficacy of self-healing coatings [11].

Damaged and undamaged samples were embedded in concrete and tested for corrosion resistance by accelerated corrosion testing. Results from Chen *et al.* showed that reinforcement with experimental coatings had times to failure three times longer than conventional coated reinforcement. Furthermore, after 150 days, 83% of the self-healing samples still exhibited no

corrosion. However, there was no difference in time to failure observed between undamaged and damaged coatings, suggesting that the procedure did not create enough damage to significantly induce greater corrosion. This result also suggests that the increased time to failure of the experimental coatings could be a result of thicker experimental coatings controlled by the incorporation of microcapsules [11].

Carpenter and Loucks (2016) conducted further research [31]. The purpose of this investigation was to assess the performance of the self-healing coatings under harsher impact and cut damaging conditions. Similarly, experimental and control coated rebar samples were damaged, embedded in concrete, and subjected to accelerated corrosion testing. Results showed that undamaged experimental coatings had the longest time to failure, followed by experimental cut and impact damaged samples, respectively. Control coatings had less than half the time to failure of experimental coatings, with cut damaged control coatings lasting the longest of the group followed by undamaged and impact damaged control coatings, respectively [31]. These results suggest the potential advantages of self-healing coatings on reinforcement; however, the results had high standard deviations. Additionally, there may not have been harsh enough damaging conditions as the damaged control coatings lasted longer than the undamaged control samples. Furthermore, coating thickness was evaluated as an increase in diameter compared to the diameter of uncoated reinforcement. Results showed that the thicknesses were similar amongst uncoated, control, and experimental coatings [31]. This result conveys that the varying geometry of reinforcement may make it difficult to assess the coating thickness, as surely, uncoated reinforcement would have a smaller diameter compared to coated reinforcement.

This thesis intended to continue research on self-healing coatings for steel reinforced infrastructure while investigating some of the results obtained from previous studies, specifically, the research by Chen *et al.* and Carpenter and Loucks. To this end, self-healing and experimental coatings were produced on steel coupons so that the mechanical and corrosion resistance properties of the coatings could be studied on a less variable flat surface. Coatings were applied to coupons, coating thicknesses were measured, samples were damaged, and adhesion and corrosion resistance was evaluated periodically after submersion in an aerated salt-water bath.

3.0 Methodology

To fulfill the goal of this research, multiple procedures were conducted on several sample types. The figure below outlines the methodology by displaying the processes, in numbered order, and the samples that were created and subjected to the various studies (Figure 9). The subsequent sections further detail the methodology.

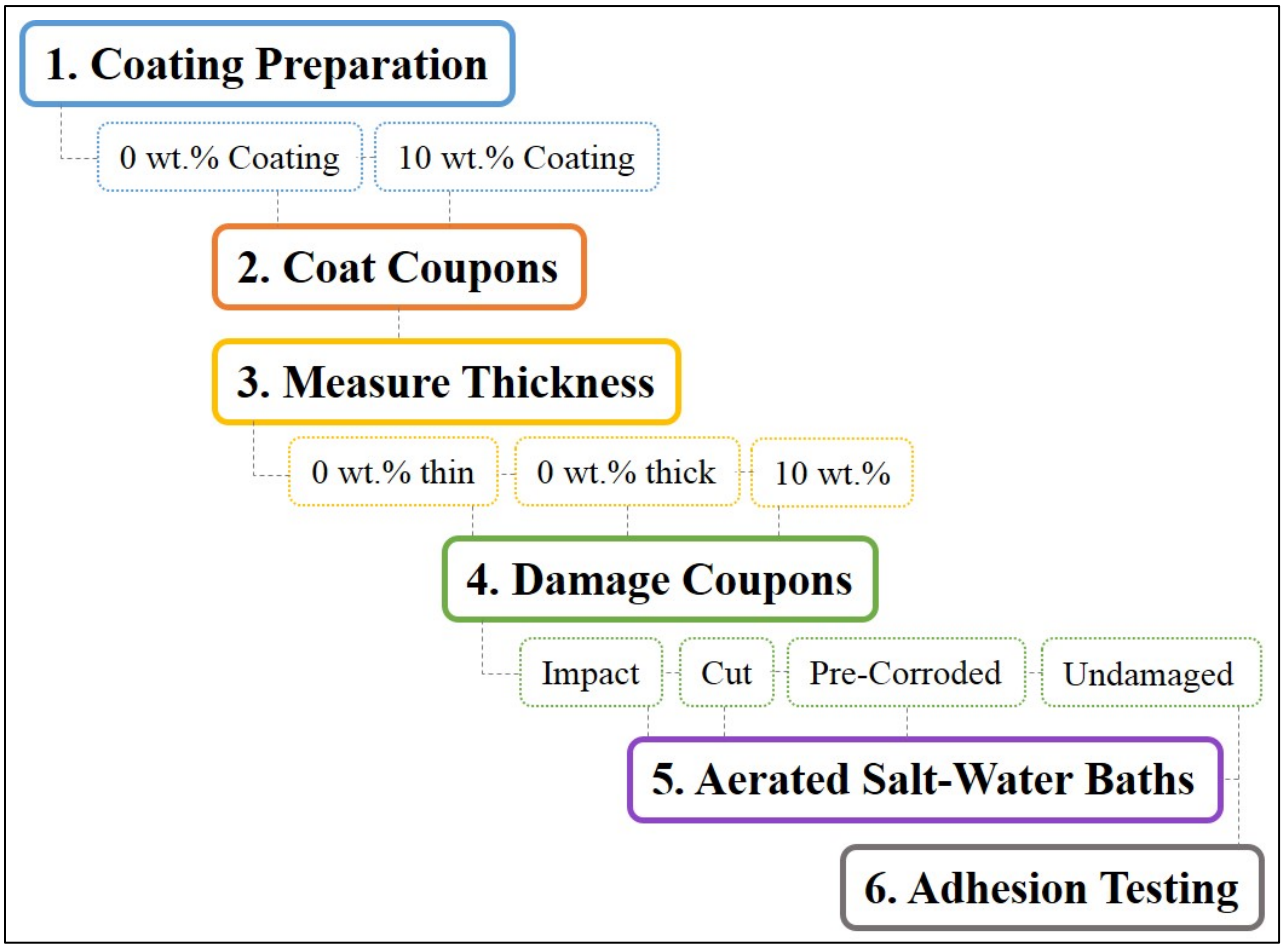

Figure 9: Outline of the methodology detailing the various processes and samples that were created and investigated.

3.1 Coating Preparation

Microcapsules remaining from the investigation by Carpenter and Loucks were utilized for this study. The microcapsules were created through an emulsion process based on the procedure by Samadzadeh *et al* [32] to encapsulate tung oil (Table 2). The microcapsules had a broad size distribution with a mean diameter of 0.013 ± 0.003 in (0.343 ± 0.093 mm) [31]. Microcapsules were combined with a two-part epoxy to create a 10 wt.% self-healing coating. Epoxy resin and microcapsules were mixed in a planetary centrifugal mixer at 200 rpm for two minutes and degassed for 30 seconds at 400 rpm. Epoxy activator was then added to the resin-microcapsule combination, mixed for three minutes, transferred to a new container, and mixed for three more minutes. Epoxy coatings were produced using the same two-part epoxy, without the addition of microcapsules.

Table 2: Properties of tung oil [33]

Form	Liquid
Composition	Ester of eleostearic acid, esters of linolenic, 9, 12-linoleic, oleic, stearic and palmitic acids
Color	Colorless to yellow to brown
Specific Gravity at 77°F (25°C)	0.930-0.940

3.2 Steel Coupon Coating and Damage

Coatings were applied to 3 in x 5 in x 0.032 in (76.2 mm x 127 mm x 0.8 mm) steel coupons designed to comply with ASTM B117. Before coating, all coupons were taped around the edges using a water resistant adhesive tape. The thickness of this border was measured using calipers to ensure consistent thickness among all coupons. Coatings were poured onto the coupons and leveled using a plastic squeegee and the tape as a guide for thickness control. Coatings were applied to one side at a time and given 72 hours to cure, per manufacturer recommendation.

Coating thickness was measured after coating one side of the coupon. Ten thickness measurements were taken per sample using calipers. Afterwards, the confirmed manufacturer thickness of the substrate was subtracted from the measurements and the coating thickness values were obtained. With both sides coated, another ten thickness measurements per sample were taken. From these measurements, the average of the previously measured thickness of each sample was subtracted to obtain the coating thickness of the second side. A one-way analysis of variance (ANOVA) was conducted between the coating thicknesses of self-healing and epoxy coatings. Since coating thickness affects corrosion resistance, with increased thickness providing more protection, the results of the ANOVA were used to evaluate this variable.

Three coating types were created for this study: two unmodified epoxy coatings and one self-healing coating. The two unmodified coatings had varying thicknesses with one thinner and another similar in thickness to the self-healing coatings. These epoxy coated samples were used to study the effects of coating thickness on corrosion resistance. The epoxy coatings are referred to as 0 wt.% thin and 0 wt.% thick, and the self-healing coating is referred to as 10 wt.%.

For each coating type three samples were cut damaged and another three were impact damaged. A utility knife was used to create 3-in (7.62 cm) long cuts, penetrating the coating to the substrate on one side of each sample. An Instron Dynatup 8250 was used to impact damage samples. A 1-in (2.54 cm) diameter spherical tip impactor was suspended 3-in (7.62 cm) above the samples and dropped with an 11 lb (5 kg) weight. Samples were given three days to heal before further testing.

Chen *et al.* observed that impact damage yielded harsher results on self-healing coatings compared to unmodified epoxy coatings. For this reason, after the self-healing coatings were applied to the coupons and impact damaged, fragments of the debonded coating were imaged using Scanning Electron Microscopy (SEM). These images were obtained using a 3.0 kV beam voltage, a probe current of 3, and a working distance of 0.394 in (10 mm). SEM was used to inspect the regions surrounding microcapsules to try and justify the damage of the impacted 10 wt.% samples.

Additionally, samples were damaged by pre-corroding the substrate and then applying a coating. Pre-corroded samples were created to assess the coatings' ability to inhibit further corrosion on samples that had already begun to corrode, mimicking a situation in which a coating is applied over an unnoticed corrosive area. Theses samples were created by placing approximately 0.034 oz (1 mL) of 5 wt.% sodium chloride onto one side of the uncoated substrate. The droplet was given three days to corrode, over which time the water in the solution evaporated and left a deposit of sodium chloride on the surface. The substrates were brushed clean of sodium chloride and coatings were applied to the coupons. Since the coating thicknesses were not measured for these samples, only 0 wt.% and 10 wt.% coatings were used.

For each coating type, a total of 24 samples were created (Table 2). Three samples were created with impact damage, three with cut damage, and three with pre-corrosion damage. Additionally, 18 samples were created, undamaged, to be used three at a time in weekly intervals for adhesion testing.

Table 3: Table displaying all samples created and the respective damage.

Coating Type	Damage Type			Undamaged
	Impacted	Cut	Pre-Corroded	
0 wt.% thin	3 samples	3 samples	3 samples	18 samples
0 wt.% thick	3 samples	3 samples		18 samples
10 wt.%	3 samples	3 samples	3 samples	18 samples

3.3 Aerated Salt-Water Baths

All samples for each coating type were submerged in 5 wt.% sodium chloride solution with an aerator, creating a corrosive aerated salt-water bath. As the steel substrates corroded and rust accumulated, the mass of the samples increased. Therefore, samples were periodically monitored in the aerated salt-water baths by weighing and photographing. The weight measurements were plotted and fit with linear trend lines for each coating type. The slopes of these lines were used as quantitative analysis of the rate of corrosion with the R^2 value used as a measure of fit for the linear regression. Photographs of the samples were used for qualitative analyses, displaying the progression of corrosion.

3.4 Adhesion Strength

Chen *et al.* noted that self-healing coatings delaminated near the damage regions, suggesting decreased adhesion strength of these coatings. Therefore, this study evaluated the adhesion of 0 wt.% (thin and thick) and 10 wt.% coatings to the steel substrate in accordance with ASTM D3359 Test Method B. Briefly summarized, six parallel 0.75-in (20 mm) long cuts spaced 0.08 in (2 mm) apart were made using a utility knife, paying particular attention to cutting through the coatings down to the substrate. Another six cuts were made perpendicular to these cuts to create a 25 square grid. The surface was wiped clean of any detached particles, and a 3-in (7.62 cm) long piece of ASTM D3359- certified tape was placed over the grid. The tape was manually smoothed until the adhered area of the tape was uniformly colored, representing a consistent bond over the grid and no entrapped air. After 90 seconds, the tape was removed at an approximate 180° angle to the substrate in a single, gentle pull. The adhesion of the coatings was determined by visually analyzing the grid for delamination and debonded area, and assigning the appropriate ASTM D3359 rating (Table 4). Three samples for each coating type were tested each week for adhesion

after being submerged in the aerated salt-water baths. Three adhesion tests were conducted per sample on one side, totaling nine adhesion results per week, per coating type (Figure 10).

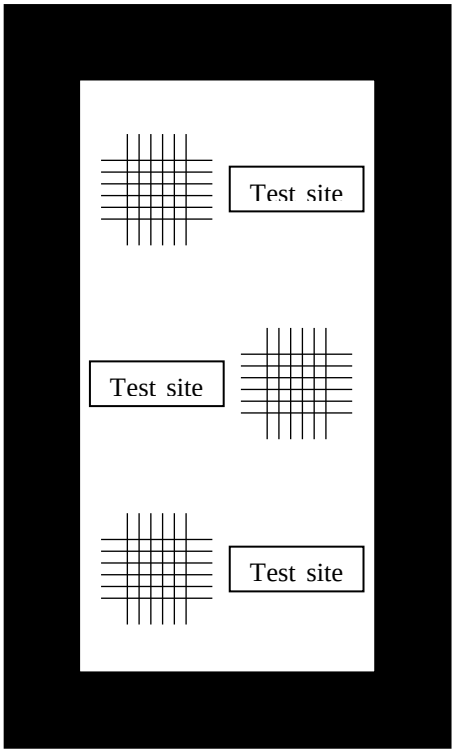

Figure 10: Schematic of adhesion samples displaying the three testing sites per sample

Table 4: ASTM D3359 Test Method B Classifications [34]

CLASSIFICATION OF ADHESION TEST RESULTS		
CLASSIFICATION	PERCENT AREA REMOVED	SURFACE OF CROSS-CUT AREA FROM WHICH FLAKING HAS OCCURRED FOR SIX PARALLEL CUTS AND ADHESION RANGE BY PERCENT
5B	0% None	
4B	Less than 5%	
3B	5 – 15%	
2B	15 – 35%	
1B	35 – 65%	
0B	Greater than 65%	

4.0 Results and Discussion

4.1 Coating Thickness

Coating thickness can affect the corrosion resistance of a sample. Theoretically, a thicker coating will have better performance over a thinner coating, since thicker coatings will provide a longer distance for diffusion for aggressive media. Therefore coating thickness was measured before assessing the corrosion resistance performance of samples to better understand the variables affecting the results. Three coating types were prepared; a 10 wt.% self-healing coating and two 0 wt.% coatings; one with a thickness less than the 10 wt.% coatings and one with comparable coating thickness to the 10 wt.% coating. These unmodified epoxy coatings, referred to as 0 wt.% thin and 0 wt.% thick, respectively, were created to investigate whether self-healing coatings have improved corrosion resistance, compared to unmodified coatings, independent of the coating thickness.

The average coating thickness of 0 wt.% thin samples was 0.007 ± 0.004 in (0.18 ± 0.10 mm) per side. The average thickness of 0 wt.% thick samples was 0.013 ± 0.006 in (0.33 ± 0.152 mm) per side. The relatively high standard deviation for 0 wt.% coatings was believed to be a result from too much pressure applied to 0 wt.% thin samples and variable pressure applied to 0 wt.% thick samples while regulating the coating thickness with the squeegee. The average coating thickness of 10 wt.% samples was 0.012 ± 0.003 in (0.31 ± 0.076 mm) per side. It was observed that the thickness of the 10 wt.% coatings was similar to the median microcapsule diameter documented by Carpenter and Loucks (2016) and small peaks formed at the location of microcapsules. This suggests that the 10 wt.% coating thicknesses are dependent on the size of the microcapsules and therefore lead to increased thickness (Figure 11).

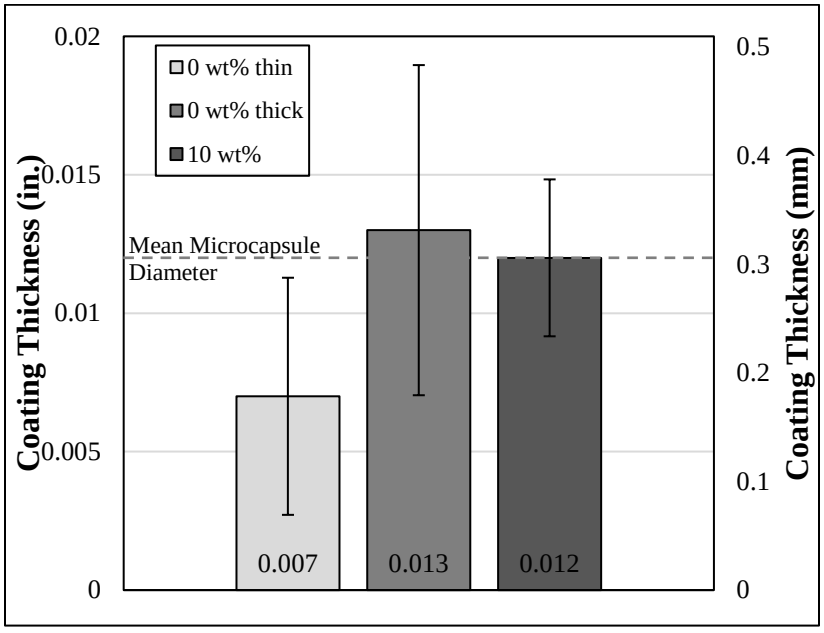

Figure 11: This graph compares the average coating thicknesses for the different samples. Also graphed is the mean microcapsule diameter to compare with the 10 wt.% samples.

There was a statistically significant ($p < 0.05$) difference between the 0 wt.% thin and 10 wt.% coating thicknesses, with the 0 wt.% thin coating 42% thinner than the 10 wt.% coating. Similarly,

there was a difference between the 0 wt.% thick and 10 wt.% coating thicknesses. However, the 0 wt.% thick coatings were 7.7% thicker than the 10 wt.% coatings. Although there is a difference in coating thicknesses for the 0 wt.% thick and 10 wt.% samples, the difference was considered negligible and insignificant.

4.2 Adhesion Strength

Adhesion was tested weekly after samples were submerged in aerated salt-water baths. Results from testing conducted at day zero suggest that 0 wt.% thin samples had better adhesion to the substrate over 0 wt.% thick and 10 wt.% samples. After one week of submersion, all coatings performed similarly, displaying poor adhesion to the substrate (Figure 12).

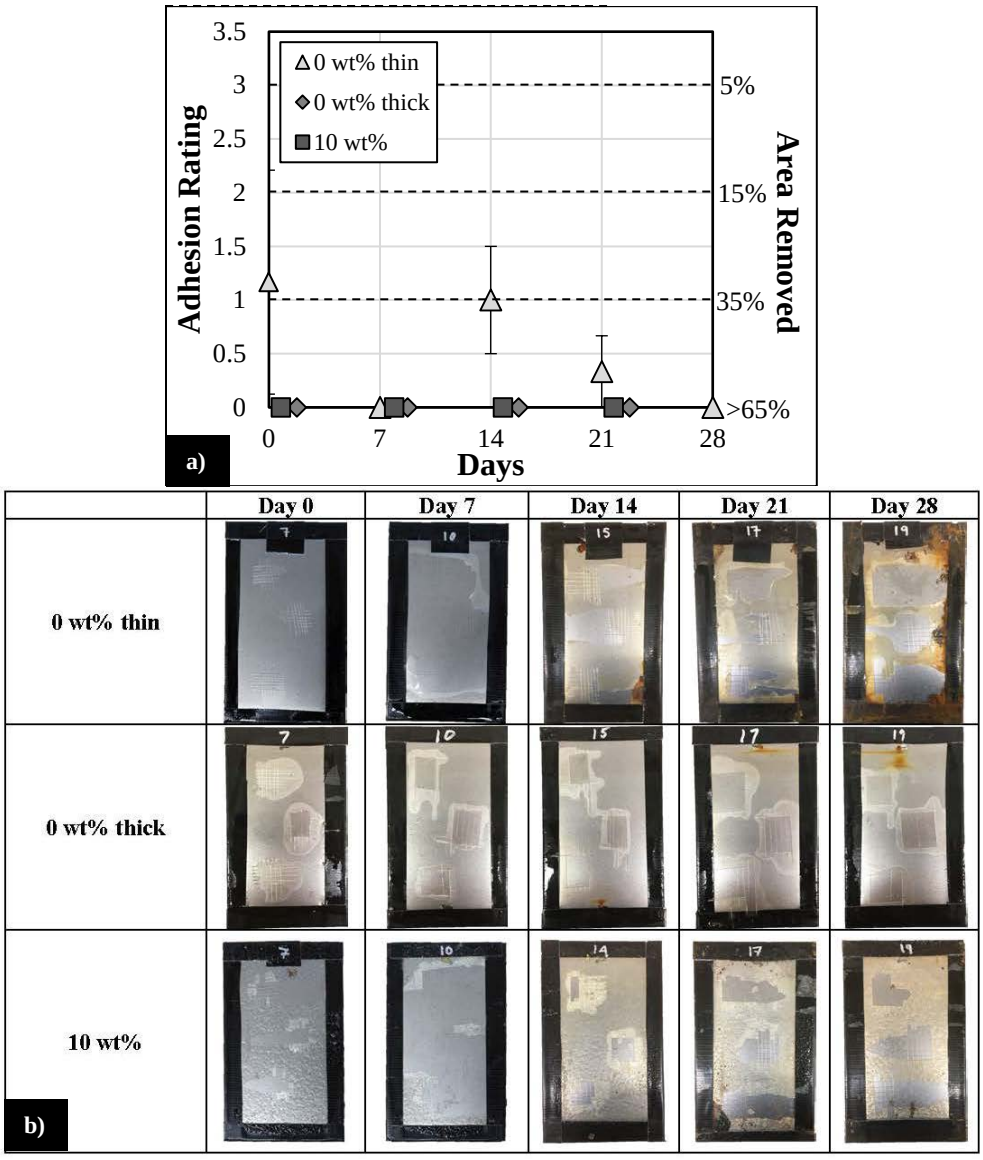

Figure 12: Adhesion of 0 wt.% thin, 0 wt.% thick, and 10 wt.% coatings to metal substrate. A) ASTM D3359 rating and corresponding area removed vs. the number of days in the salt water bath. Note samples were tested on a weekly basis and data points are offset as to not overlap. B) Qualitative results from the adhesion tests at 7-day intervals with three adhesion tests conducted on one side per sample.

While 0 wt.% thin samples had better initial adhesion to the substrate, the adhesion was variable each week with high standard deviations. This is likely due to the inconsistent coating thickness of 0 wt.% thin samples with increased adhesion in regions with thinner coatings and decreased adhesion with thicker coatings, as was observed in the 0 wt.% thick samples (Figure 12). The poor adhesion of 10 wt.% coatings could be a result of the microcapsules acting as imperfections at the interface between the coating and the substrate. However, no statistically significant difference ($p < 0.05$) was observed in adhesion to steel coupons between all coatings. This result suggests that 0 wt.% and 10 wt.% coatings have poor adhesion to the substrate, independent of coating thickness and incorporation of microcapsules.

Poor adhesion is a property of coatings that can lead to the corrosion of reinforcement. An inadequate bond between the coating and the substrate can cause the coating to flake off, providing no protection from the environment. The ideal coating to protect reinforcement from corrosive media needs to have even and consistent adhesion. This is a property that needs to be optimized for self-healing coatings to be adopted for industry use.

4.3 Aerated Salt-Water Baths

All samples were submerged in aerated salt-water baths and monitored periodically to analyze the progression of corrosion. Impact damaged 0 wt.% thin samples displayed a rate of corrosion of 0.003 oz./day (83 mg/day). 0 wt.% thick samples corroded at 0.001 oz./day (38 mg/day). The 10 wt.% samples corroded at 0.005 oz./day (147 mg/day) (Figure 13). 10 wt.% samples had the least corrosion resistance, quantitatively and qualitatively, among all impact damaged samples, followed by 0 wt.% thin and 0 wt.% thick samples, respectively. 0 wt.% thin coatings had a low R^2 value which is possibly a result of the variably thin areas of coating corroding more than thicker regions (Figure 14).

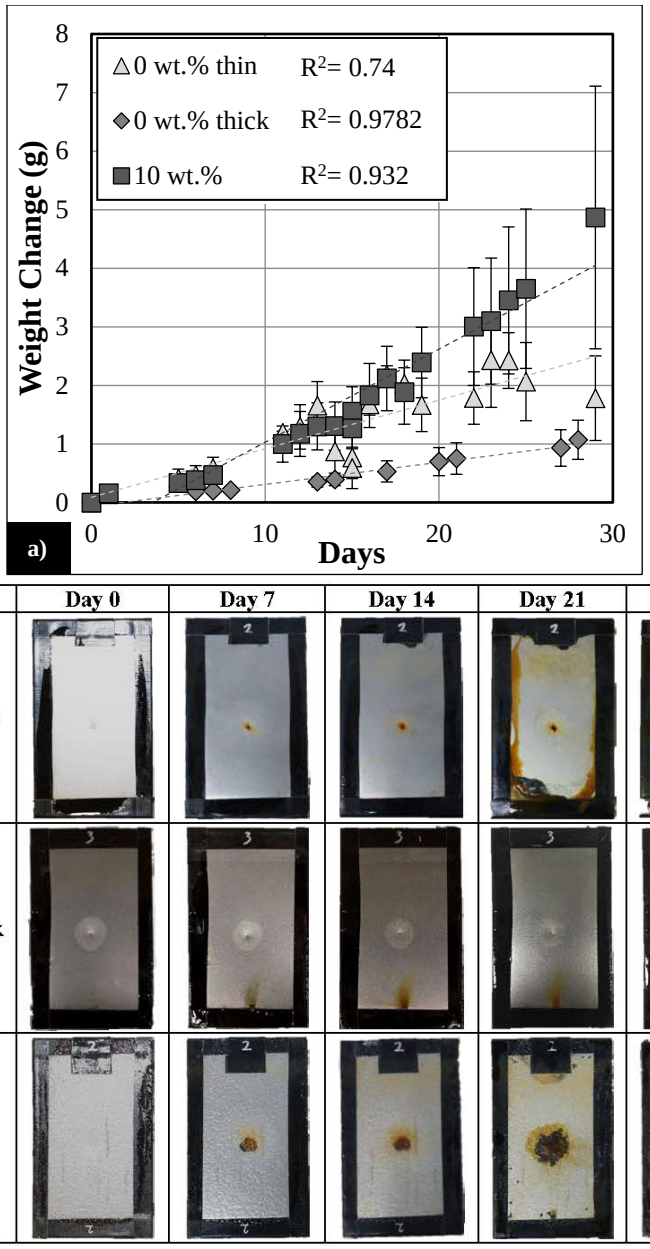

Figure 13: Analysis of impact damage samples for 0 wt.% thin, 0 wt.% thick, and 10 wt.% samples. a) Quantitative results of rust accumulation on samples measured by increase in sample weight with time b) Qualitative results of rust accumulation.

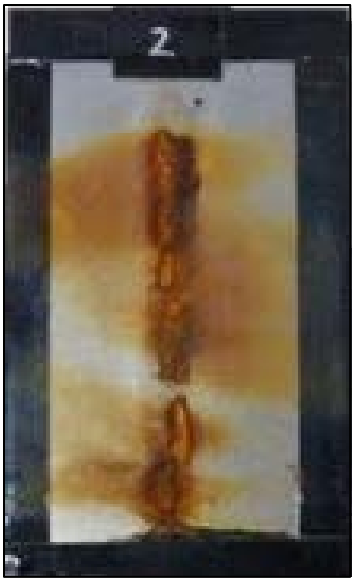

Figure 14: Common rust formulation on 0 wt.% thin samples where squeegee was used with too much pressure leading to thinner coatings in the center of the samples and the accumulation of rust.

It was visually observed that impacting 10 wt.% coated samples resulted in harsher damage of the coatings compared to 0 wt.% samples. 10 wt.% coatings debonded from the substrate and fractured causing fragments to detach from the samples, whereas 0 wt.% samples only debonded from the substrate (Figure 15).

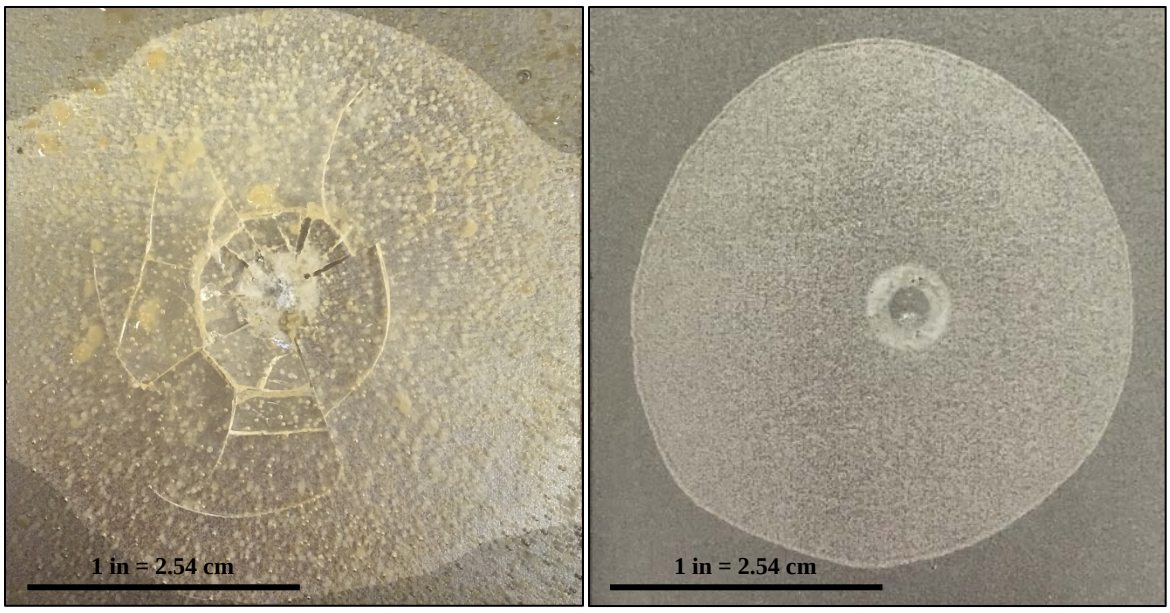

Figure 15: Impact damage observed on a) 10 wt.% samples and b) 0 wt.% samples. a) shows the debonded and fractured regions of the 10 wt.% coatings and b) shows the debonded regions of the 0 wt.% coatings.

Fragments of detached 10 wt.% coatings were collected and imaged via SEM to try to understand the brittle fracture of the 10 wt.% coatings when impact damaged. It was observed that there were small cracks propagating from particles in the coating roughly 0.0001 in. (3μm) in diameter. These cracks were an average of 0.001 ± 0.0002 in. (0.025 ± 0.006 mm) long with varying thickness along the length to the crack (Figure 16).

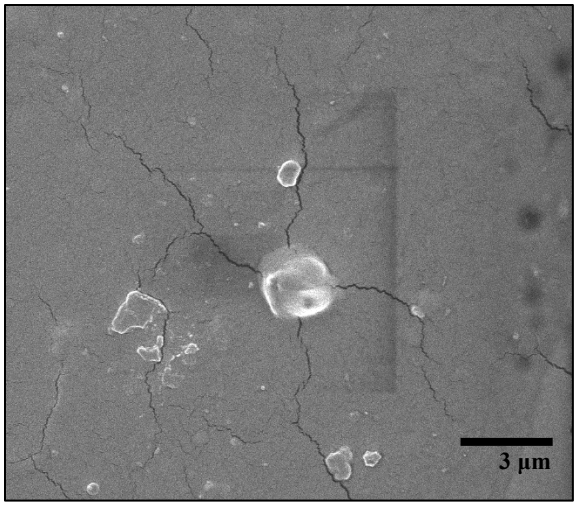

Figure 16: SEM image of 10 wt.% coating fragments showing four cracks propagating from a microcapsule

Based on the fundamentals of linear elastic fracture mechanics, this scenario depicts a Mode I fracture, in which the crack tip opens and propagates until failure. When the 10 wt.% coatings are impacted, the particles are compressed, increasing the diameter of the cross section. This expansion causes tensile stresses that open cracks, causing them to propagate to brittle fracture. This finding of initial cracks near particles in 10 wt.% coatings provides a potential explanation for the unique fracture of these coatings and subsequent inability to heal the damaged area, leading to decreased corrosion resistance, compared to 0 wt.% coatings.

Cut damaged 0 wt.% thin samples corroded at a rate of 0.004 oz./day (107 mg/day), whereas 0 wt.% thick samples corroded at 0.001 oz./day (33 mg/day). Cut damaged 10 wt.% samples corroded at a rate of 0.002 oz./day (70 mg/day). Quantitatively, 0 wt.% thick samples had the most corrosion resistance followed by 10 wt.% and 0 wt.% thin samples, respectively (Figure 17a). However, qualitatively, 0 wt.% thick and 10 wt.% samples show similar accumulation of rust near the cut damaged regions (Figure 17b). Analysis of the 10 wt.% samples showed a slight accumulation of rust forming at the boundary of tape and coated substrate. Since more corrosion increases the weight of the samples, this could provide an explanation as to why the quantitative results suggest the 10 wt.% samples have less corrosion resistance than 0 wt.% thick samples. Similarly, 0 wt.% thin samples had rust accumulation at the tape-coating boundary. This is likely why the 0 wt.% thin samples have a low associated R^2 value and high standard deviation for the data.

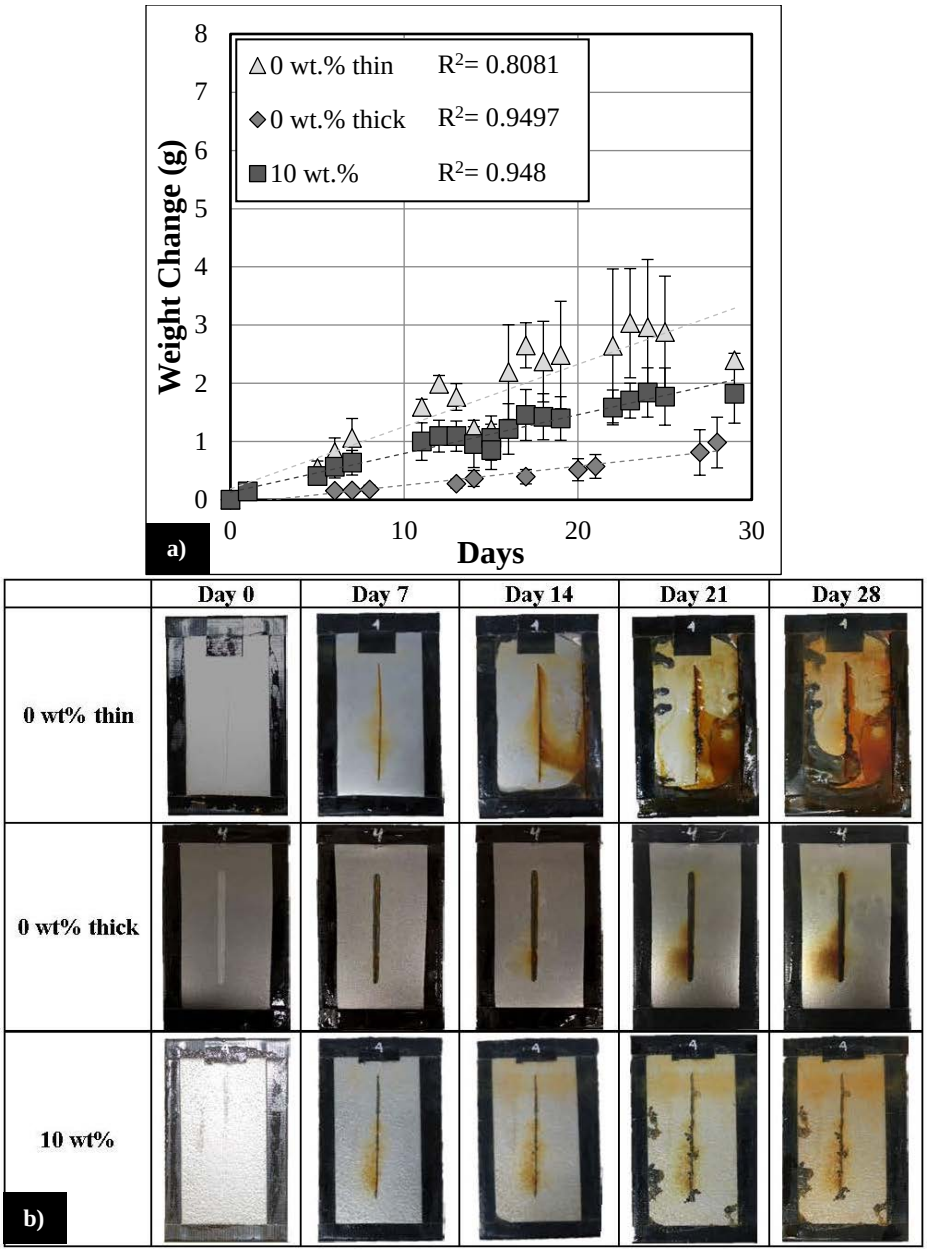

Figure 17: Analysis of cut damage samples for 0 wt.% thin, 0 wt.% thick, and 10 wt.% samples. a) Quantitative results of rust accumulation on samples measured by increase in sample weight with time b) Qualitative results of rust accumulation.

Undamaged 0 wt.% thin coatings had a rate of corrosion of 0.003 oz./day (91 mg/day). 0 wt.% thick coatings corroded at 0.0008 oz/day (24 mg/day). Undamaged 10 wt.% coatings corroded at a rate of 0.0005 oz./day (15 mg/day) (Figure 18). Undamaged 0 wt.% thick and 10 wt.% samples performed similarly, quantitatively and qualitatively. These results suggest that 0 wt.% thin samples had poor corrosion resistance, however there was a high standard deviation in the quantitative data for these samples, which resulted in a low R^2 value. From the qualitative analysis of 0 wt.% thin samples, it was noticed that there was once again corrosion at the tape-coating interface likely causing the variance in data for 0 wt.% thin samples. Undamaged 10 wt.% samples

had an unusually low R^2 value given the apparent linearity of the data. There is no immediate explanation for this result.

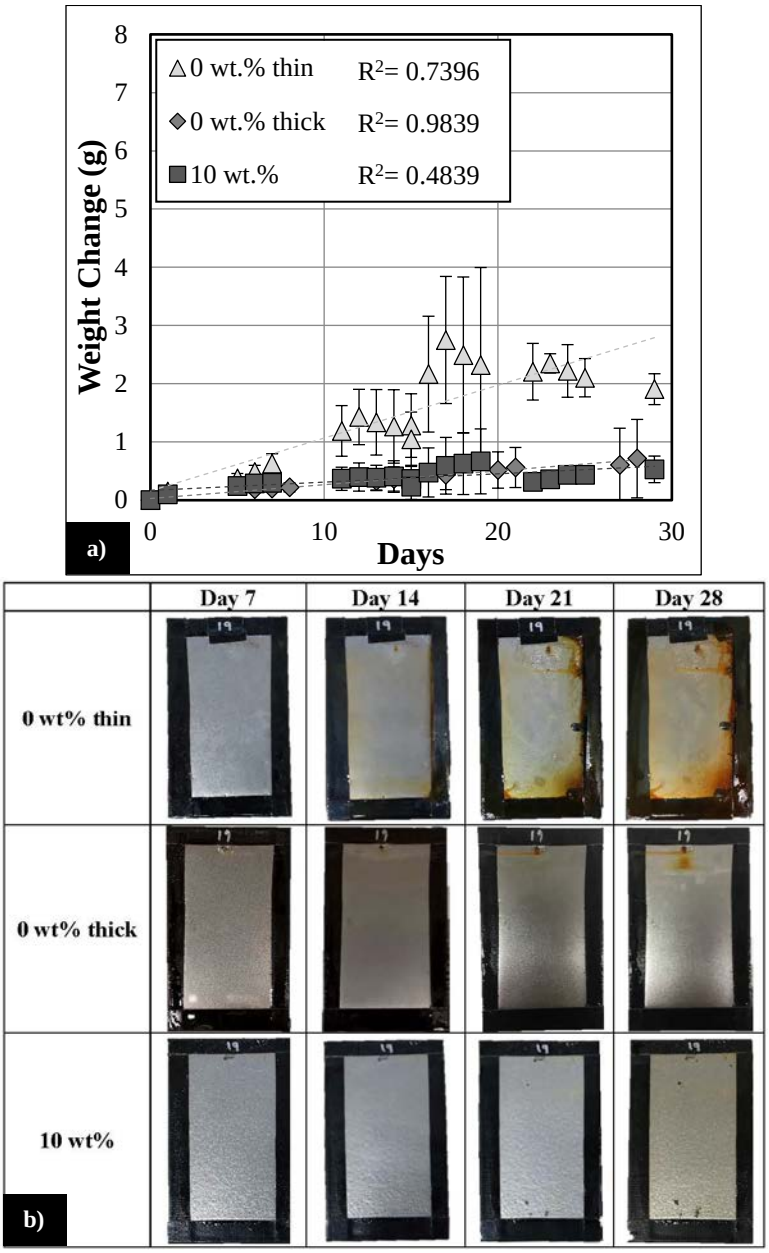

Figure 18: Analysis of undamaged samples for 0 wt.% thin, 0 wt.% thick, and 10 wt.% samples. a) Quantitative results of rust accumulation on samples measured by increase in sample weight with time b) Qualitative results of rust accumulation.

Pre-corroded samples were created to analyze the performance of 0 wt.% and 10wt.% coatings when applied over undetected corrosion. Quantitative results from the pre-corroded samples submerged in the aerated salt-water baths suggest that 10 wt.% samples corroded at a slower rate than the conventional coatings (Figure 19). 0 wt.% coatings corroded at a rate of 0.0045 oz./day (127 mg/day) and 10 wt.% coatings displayed a rate of corrosion of 0.002 oz./day (56 mg/day). However, qualitative analysis of the samples display increased corrosion in 10 wt.% samples. 0

wt.% coatings contained the corrosion local to the pre-corrosion, whereas the 10 wt.% coatings began to show an unusual stippling pattern. The origins of this pattern are not immediately clear, and require further research. It was believed that there was corrosion behind the tape of the 0 wt.% samples, caused by low adhesion at the tape-coating boundary, that was qualitatively unobservable, however, influenced the quantitative results.

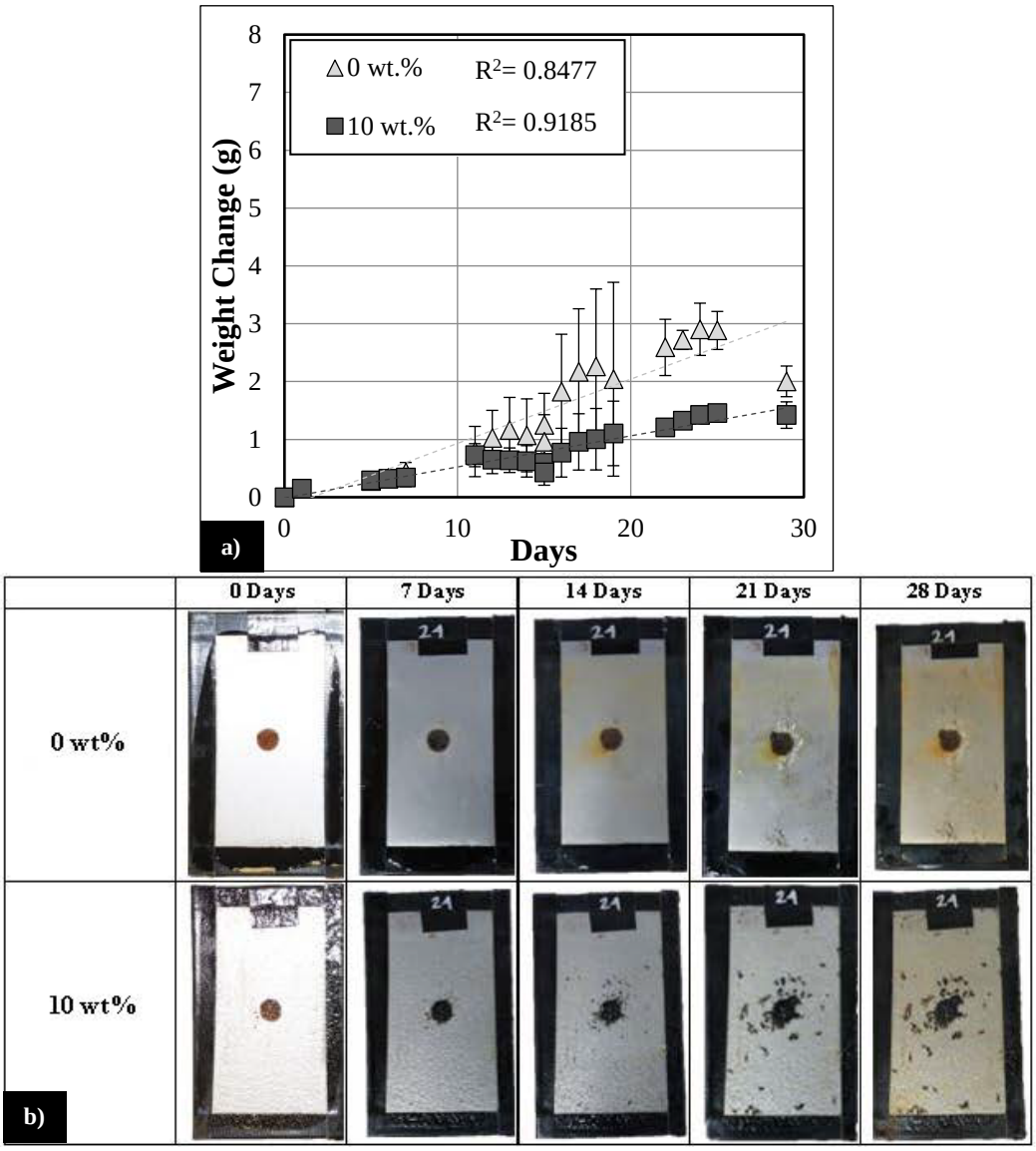

Figure 19: Analysis of pre-corroded samples for 0 wt.% and 10 wt.% samples. a) Quantitative results of rust accumulation on samples measured by increase in sample weight with time b) Qualitative results of rust accumulation. Note unusual stippling pattern on 10 wt.% samples most pronounced at 28 days.

5.0 Conclusion

This study identified the potential for improved corrosion resistance of steel reinforced infrastructure with the application of self-healing epoxy coatings. 10 wt.%, 0 wt.% thin, and 0 wt.% thick coatings were applied to steel coupons, damaged, and assessed for adhesion strength and corrosion resistance at weekly intervals. Results showed that adhesion strength was similar with all coatings having limited adhesion to the substrate. Corrosion resistance varied depending on the coating and incurred damage. Compared to 0 wt.% thin coatings, 10 wt.% samples had improved corrosion resistance for cut, undamaged, and pre-corroded samples. 10 wt.% samples had similar corrosion resistance to 0 wt.% thick coatings for cut and undamaged samples. 10 wt.% impact damaged samples were damaged beyond their healing ability, likely due to initial cracks near microcapsules. This damaged decreased the corrosion resistance of impacted 10 wt.% samples.

Previous studies investigating self-healing coatings for steel reinforced infrastructure suggested that the mechanical properties of structural concrete were unaffected by the incorporation of microcapsules, unlike the diminished bond strength of galvanized and FBE coatings. Furthermore, it is well established that epoxy coatings are more economical than other corrosion mitigation techniques, such as stainless steel. However, previous investigations questioned the reliability of self-healing coatings for corrosion protection. Results from this study demonstrated that self-healing coatings have increased corrosion resistance due to their self-healing ability, however, they have poor adhesion to the substrate. While these results are promising, a protective coating needs to have adhesion to the substrate to be reliable and ensure protection.

There are numerous avenues for future research investigating self-healing coatings for steel reinforcement. These include modifications to this study. The samples in this investigation were prepared via a manual process that could have led to variations in the samples such as coating thicknesses and corrosion at the tape-coating boundary. Future investigations could utilize a less manual processes, such as spray coatings, to have more control during coating preparation. Additionally, research could be conducted in continuation of this study to improving the adhesion strength of self-healing coatings to the substrate and reducing cracks within the cured coatings. Adhesion could be tested on reinforcement, rather than coupons, to evaluate whether the geometry of the reinforcement leads to increased adhesion of the coating. Also, microcapsule size could be varied by modifying the synthesis conditions to find the optimal size distribution to maximize the service life. Furthermore, adoption of this method could be more likely if there was more analysis and imaging of the self-healing action of these coatings. Lastly, research should be conducted to augment the current FBE coating process with microcapsules for easy adoption in industry.

The corrosion of steel in infrastructure is estimated to cause around $276 billion each year in direct costs. Additionally, American motorists lose a total of 4.2 billion hours every year due to maintenance-related congestion and waste 3.9 billion gallons of fuel. Furthermore, lives are lost each year from deteriorating infrastructure with an estimated 33% of traffic fatalities caused by roadway features. This research lead to an understanding of the fundamental mechanisms governing self-healing coating performance in infrastructure applications, increasing the service life of steel reinforcement and therefore decrease the yearly costs of infrastructure maintenance, travel time for motorists, resources consumed and wasted, and improve user safety.

6.0 References

[1] Emmons, P. H., & Sordyl, D. J. (2006). The State of the Concrete Repair Industry, and a Vision for its Future. *Concrete Repair Bulletin , 19* (4), 7-14.

[2] U.S. DOT Federal Highway Administration. (2017). *National Bridge Inventory*. Retrieved from Bridges & Structures: https://www.fhwa.dot.gov/bridge/nbi.cfm

[3] ASCE. (2017). *A Comprehensive Assessment of America's Infrastructure*. Retrieved from 2017 Infrastructure Report Card: http://www.infrastructurereportcard.org/

[4] Virmani, Y. P., & Clemena, G. G. (1998). *Corrosion Protection Concrete Bridges.* Federal Highway Administration.

[5] Holth, N. (2013). *Alvord Lake Bridge.* Retrieved from Historic Bridges: http://historicbridges.org/bridges/browser/?bridgebrowser=california/alvordlake/

[6] Watkins, C. (2006). *The Historic Devil's Elbow Bridge Is In Need Of Repair*. Retrieved from Conor Watkins' Ozark Mountain Experience: http://www.rollanet.org/~conorw/cwome/article51&52combined.htm

[7] Kepler, J., Darwin, D., & Locke, C. J. (2000). *Evaluation of Corrosion Protection Methods for Reinfroced Concrete Highway Structures.* University of Kansas Center for Research, Inc. Structural Engineering and Engineering Materials.

[8] Behzadnasab, M., Mirabedini, S., Esfandeh, M., & Farnood, R. (2017). Evaluation of Corrosion Performance of a Self-Healing Epoxy- Based Coating Containing Linseed Oil-Filled Microcapsules via Electrochemical Impedence Spectroscopy. *Organic Coatings, 105*, 212-224.

[9] Zheludkevich, M., Tedim, J., & Ferreira, M. (2012). "Smart" Coatings for Active Corrosion protection Based on Multi-Functional Micro and Nanocontainers. *Electrochimica Acta, 82*, 314-323.

[10] Montemor, M. (2014). Functional and Smart Coatings for Corrosion Protection: A Review of Recent Advances. *Surface and Coatings Technology, 258*, 14-37.

[11] Chen, Y., Xia, C., Shepard, Z., Smith, N., Rice, N., Peterson, A., et al. (2017). Self-Healing Coatings for Steel-Reinforced Concrete. *ACS Sustainable Chemistry & Engineering, 5* (5).

[12] Hassoun, M., & Al-Manaseer, A. (2015). *Structural Concrete; Theory and Design.* John Wiley & Sons, Incorporated.

[13] Portland Cement Association. (2017). *Corrosion of Embedded Metals*. Retrieved from Portland Cement Association: http://www.cement.org/learn/concrete-technology/durability/corrosion-of-embedded-materials

[14] Zhao, Y., & Jin, W. (2016). *Steel Corrosion-Induced Concrete Cracking.* Elsevier.

[15] Nurnberger, U. (2005). Stainless Steel in Concrete Structures. In H. Bohni (Ed.), *Corrosion in Reinforced Concrete Structures.* Cambridge, England: Woodhead Publishing Limited.

[16] The Institute of Materials. (1996). *Stainless Steel in Concrete: State of the Art Report.* European Federation of Corrosion Publications.

[17] Tylek, I., & Kuchta, K. (2014). Mechanical Properties of Structural Stainless Steels. *Technical Transactions: Civil Engineering*, 4-B.

[18] International Zinc Association. (2006). Hot Dip Galvanized Reinforcing Steel: A Concrete Investment. Brussels.

[19] Hunkeler, F. (2005). Corrosion in Reinforced Concrete: Processes and Mechanisms. In H. Bohni (Ed.), *Corrosion in Reinforced Concrete Structures.* Cambridge, England: Woodhead Publishing Limited.
[20] Manning, D. (1996). Corrosion Performance of Epoxy-Coated Reinforcing Steel: North American Experience. *Construction and Building Materials, 10* (5), 17.
[21] Scan India. (2006). *Fusion Bonded Epoxy Coating*. Retrieved from Scan India: http://www.scanpipes.com/img/fusion-bonded-epoxy-coating3.jpg
[22] NACE. (2013). *Highways and Bridges*. Retrieved from NACE International: https://www.nace.org/Corrosion-Central/Industries/Highways-and-Bridges/
[23] Bertolini, L., Elsener, B., Pedeferri, P., Redaelli, E., & Polder, R. B. (2013). *Corrosion of Steel in Concrete: Prevention, Diagnosis, Repair* (2 ed.). Weinheim, Germany: John Wiley & Sons, Inc.
[24] Cho, S. H., White, S., & Braun, P. (2009). Self-Healing Polymer Coatings. *Advanced Materials, 21*, 4.
[25] Ghosh, S.K. (2009). Self-healing Materials: Fundamentals, Design Strategies, and Applications. In S.K. Ghosh (ed.), *Self-Healing Materials: Fundamentals, Design Strategies, and Applications.* Weinheim: Wiley-VCH Verlag GmbH & Co. KGaA.
[26] Chen, X., Dam, M.A., Ono, K., Mal, A., Shen, H., Nutt, S.R., Sheran, K., & Wudl, F. (2002). A Thermally Re-mendable Cross-Linked Polymeric Material. *Science, 295* (5560), 1698-1702.
[27] Chen, X., Wudl, F., Mal, A., Shen, H., & Nutt, S.R. (2003). New Thermally Remendable Highly Cross-Linked Polymeric Materials. *Macromolecules, 36* (6), 1802-1807.
[28] Toohey, K.S., & Sottos, N.R. (2007). Self-healing materials with microvascular networks. *Nature Materials, 6*, 581-585.
[29] Lee, J.Y., Buxton, G.A., & Balazs, A.C. (2004). Using nanoparticles to create self-healing composites. *The Journal of Chemical Physics, 121* (11), 5531-5540.
[30] Shirinyan, A.S., & Wautelet, M. (2004). Phase separation in nanoparticles. *Nanotechnology, 15* (12).
[31] Carpenter, M., & Loucks, R. (2016). *Self-Healing Coatings for Steel-Reinforced Infrastructure.* Major Qualifying Project, Worcester Polytechnic Institute, Civil and Environmental Engineering Department, Chemical Engineering Department.
[32] Samadzadeh, M., Boura, S., Peikari, M., Ashrafi, A., & Kasiriha, M. (2011). Tung oil: An autonomous repairing agent for self-healing epoxy coatings. *Progress in Organic Coatings, 70* (4), 383-387.
[33] Sigma-Aldrich. (2018). Tung Oil. *Product Specification*. Retreived from: https://www.sigmaaldrich.com/catalog/product/aldrich/440337?lang=en&region=US
[34] ASTM Standard D3359. (2017). *Standard Test Methods for Rating Adhesion by Tape Test.* ASTM International.

7.0 Appendix

Cement Forensics Research

Concrete is one of the oldest and most popular building materials. With that, concrete is frequently used as trace evidence in forensic settings such as structural investigations and failures. Petrographic microscopy is the primary method for examination of concrete trace evidence based on the aggregates in samples. However, this method excludes the relationship between samples with dissimilar aggregates, requires large samples, and is time and resource extensive. Additionally, petrographic microscopy is semi-quantitative and heavily depends on the experience of the investigator. While this method is a reliable tool for excluding dissimilar samples, new, operator-independent, qualitative methods are needed for establishing positive relationships.

This research investigated cementitious material, rather than aggregates, as a potential method for identification. The concentration of trace elements in cement can be affected by the composition of raw materials, the use of supplementary materials and alternative fuels, and environmental regulations, among other variables. It was hypothesized that the ratios of trace elements could serve as a unique ‘fingerprint’ that could be used to identify cementitious trace evidence.

Samples of several ordinary portland cements, secured from geographically diverse facilities, were prepared through acid dissolution and investigated using Total X-Ray Fluorescence (TXRF). 18 trace elements were quantified in each sample, however, analyses indicate that only eight of these elements show the promise of being usable as a characteristic ‘fingerprint’. The following data provides the TXRF trace element compositions for 23 samples (Table 2).

Table 5: Composition of eight selected 'identification' elements in 23 different samples.

Sample ID		Trace Element Compositions							
		Ti	V	Cr	Mn	Ni	Cu	Zn	Sr
1-95	A	0.04181	0.00161	0.00239	0.01932	0.00605	0.00291	0.00943	0.03822
	B	0.04176	0.00000	0.00000	0.02321	0.00537	0.00309	0.00974	0.04265
	C	0.04178	0.00218	0.00203	0.01843	0.00427	0.00283	0.00977	0.04627
2-1	A	0.05128	0.00696	0.00353	0.02581	0.00404	0.0032	0.02695	0.03291
	B	0.06315	0.00000	0.00302	0.02638	0.00409	0.00353	0.02763	0.03168
	C	0.055	0.00655	0.00245	0.02664	0.00488	0.00339	0.02715	0.03161
3-29	A	0.06025	0.00000	0.00248	0.02802	0.00356	0.00329	0.02853	0.03042
	B	0.05268	0.00624	0.00323	0.01525	0.00221	0.00209	0.01299	0.01542
	C	0.05333	0.01302	0.00000	0.02897	0.00402	0.00358	0.02591	0.03073
4-19	A	0.06576	0.00222	0.00327	0.02451	0.00298	0.00123	0.01187	0.0527
	B	0.06731	0.0025	0.00398	0.02414	0.00000	0.00411	0.01706	0.04898
	C	0.06484	0.01353	0.00000	0.02694	0.00000	0.00449	0.01215	0.05143
5-19	A	0.13088	0.00000	0.00000	0.03906	0.00514	0.00182	0.00585	0.06559
	B	0.11814	0.00000	0.00407	0.03928	0.00501	0.00192	0.00561	0.0673
	C	0.12162	0.00000	0.00464	0.03976	0.00515	0.00168	0.00567	0.07024
6-19	A	0.04221	0.00851	0.00000	0.02082	0.00423	0.00217	0.00951	0.04873
	B	0.04322	0.00108	0.00275	0.0185	0.00417	0.00212	0.0081	0.04309
	C	0.04892	0.00217	0.00379	0.01079	0.00226	0.0013	0.00396	0.02247
7-29	A	0.05596	0.01749	0.00000	0.03155	0.00657	0.00301	0.03517	0.02511
	B	0.06136	0.00777	0.00557	0.02568	0.00514	0.00283	0.0295	0.02141
	C	0.07167	0.00805	0.00588	0.02342	0.00478	0.00231	0.02625	0.01954
8-32	A	0.03745	0.00079	0.0067	0.02073	0.00268	0.00151	0.00142	0.06692
	B	0.03837	0.00000	0.0056	0.02085	0.00284	0.0018	0.00234	0.06749
	C	0.04197	0.00000	0.00618	0.02216	0.00328	0.00165	0.00152	0.06936
10-19	A	0.07032	0.0024	0.0064	0.02301	0.0065	0.00124	0.01284	0.04717
	B	0.03756	0.00262	0.00462	0.02225	0.00405	0.00152	0.0112	0.0459
	C	0.0463	0.00282	0.00427	0.02352	0.00336	0.00143	0.01165	0.05475
12-29	A	0.0394	0.00139	0.01149	0.01837	0.00702	0.00145	0.01364	0.04811
	B	0.04474	0.0026	0.00593	0.02024	0.00321	0.00124	0.01249	0.05599
	C	0.04401	0.00206	0.00544	0.02365	0.00335	0.0016	0.01506	0.06526
13-29	A	0.04969	0.00701	0.00934	0.04968	0.00439	0.00119	0.01674	0.05353
	B	0.04667	0.00583	0.00915	0.05215	0.00559	0.00139	0.01839	0.05969
	C	0.0541	0.00718	0.00942	0.04597	0.005	0.00108	0.01661	0.051
14-29	A	0.07217	0.01379	0.00000	0.02931	0.00356	0.00119	0.01117	0.06235

Sample ID		Trace Element Compositions							
		Ti	V	Cr	Mn	Ni	Cu	Zn	Sr
15-29	A	0.07726	0.00000	0.0056	0.02803	0.00426	0.00872	0.02204	0.03156
	B	0.07527	0.00000	0.00317	0.02723	0.00424	0.00239	0.02145	0.03056
	C	0.07574	0.00000	0.00561	0.02865	0.00456	0.00247	0.02372	0.03346
16-25	A	0.0495	0.00248	0.00625	0.02323	0.00357	0.00171	0.01165	0.05177
	B	0.06466	0.00263	0.00711	0.02043	0.00377	0.00135	0.00983	0.04148
18-29	A	0.00644	0.00074	0.28054	0.0221	0.11722	0.00000	0.00218	0.00341
	B	0.00000	0.00182	0.2314	0.01528	0.07687	0.00000	0.00084	0.00089
	C	0.02682	0.00145	0.19868	0.03842	0.09128	0.00000	0.0071	0.01671
21-25	A	0.02522	0.00164	0.16402	0.02112	0.08258	0.00000	0.00433	0.01679
	B	0.0176	0.00107	0.19528	0.0216	0.10057	0.00000	0.00287	0.01151
	C	0.01915	0.00125	0.18804	0.05429	0.09797	0.00000	0.00472	0.01168
25-32	A	0.01332	0.00077	0.20196	0.02194	0.10606	0.00000	0.00152	0.01188
	B	0.02042	0.00031	0.17247	0.02144	0.08863	0.00000	0.00166	0.01931
	C	0.02342	0.00079	0.16823	0.02006	0.0872	0.00000	0.00156	0.02111
26-29	A	0.01374	0.00087	0.21003	0.02145	0.11159	0.00000	0.00305	0.00864
	B	0.01943	0.00083	0.17683	0.02107	0.09734	0.00000	0.00324	0.01114
	C	0.01618	0.00098	0.18384	0.02231	0.10484	0.00000	0.00267	0.00961
27-25	A	0.01529	0.00078	0.16161	0.02359	0.09446	0.00000	0.00686	0.01159
	B	0.01891	0.00135	0.1236	0.02417	0.07827	0.00000	0.00917	0.01568
	C	0.01429	0.00096	0.12103	0.024	0.08222	0.00000	0.00917	0.01653
28-25	A	0.02978	0.00232	0.05762	0.0238	0.03548	0.00193	0.01483	0.02848
	B	0.03436	0.00165	0.05505	0.02355	0.03651	0.00174	0.0151	0.03244
	C	0.03159	0.00229	0.03928	0.02439	0.02969	0.0014	0.01664	0.03318
29-25	A	0.05202	0.00149	0.04389	0.02436	0.03137	0.00000	0.01095	0.04196
	B	0.05193	0.0021	0.03603	0.02503	0.0266	0.0016	0.01131	0.04723
	C	0.05514	0.00133	0.04093	0.0252	0.02994	0.00197	0.01407	0.04789
30-25	A	0.03541	0.00536	0.05707	0.04119	0.03975	0.00000	0.012	0.05224
	B	0.03896	0.00566	0.04495	0.04485	0.03198	0.00152	0.01278	0.05675
	C	0.04029	0.00713	0.04311	0.04474	0.02781	0.00163	0.01239	0.05247
31-51	A	0.03123	0.00354	0.05489	0.02229	0.0399	0.00395	0.01849	0.1155
	B	0.03768	0.00366	0.04188	0.01957	0.0286	0.0042	0.01896	0.12749
	C	0.04028	0.00332	0.06946	0.02025	0.03923	0.00407	0.01518	0.09564